Electric field gradient distributions about strontium nuclei in cubic and octahedrally symmetric crystal systems

Geoffrey M. Bowers and Karl T. Mueller*
Department of Chemistry, The Pennsylvania State University, 104 Chemistry Building, University Park, Pennsylvania 16802, USA
(Received 14 January 2005; revised manuscript received 25 March 2005; published 27 June 2005)

Strontium nuclei (^{87}Sr) in natural abundance are examined with magic angle spinning (MAS) nuclear magnetic resonance (NMR) of powder samples possessing either simple cubic (SrO) or fluorite-analogue ($SrCl_2$ and SrF_2) structures. The MAS spectra of these samples reveal a sideband pattern resulting from first order quadrupolar broadening of the outer transitions brought about by imperfections in the crystal structure. These imperfections lead to a distribution of electric field gradients (efgs) that can be characterized in these cases by fitting integrated sideband intensities as a function of spectral frequency with a Lorentzian function. Strontium oxide is simple cubic and found to have an isotropic ^{87}Sr chemical shift of 340 ± 1 ppm with respect to 1 M $SrCl_2$ (aqueous) and an efg distribution with a full width at half-height (FWHH) of 50.4 ± 2.5 kHz. Strontium chloride (anhydrous) is isostructural with fluorite and was found to have a ^{87}Sr chemical shift of 45.9 ± 1.2 ppm and an efg distribution with a FWHH of 30.9 ± 1.4 kHz. Strontium fluoride is also isostructural with fluorite and had a ^{87}Sr chemical shift of -13.0 ± 1.2 ppm and an efg FWHH of 104 ± 18 kHz.

DOI: 10.1103/PhysRevB.71.224112 PACS number(s): 61.72.Hh, 61.72.Ji, 76.60.−k, 74.62.Dh

INTRODUCTION

During the production and purification of weapons-grade plutonium at the Hanford Works (1944–1987) and other DOE sites, vast quantities of high and low level liquid and solid nuclear waste were generated.[1] Much of this waste is now in the form of a highly caustic (pH $\sim$ 13–14) aqueous solution with high ionic strength and free aluminum contaminated with numerous fission products, one of the most prevalent being ^{90}Sr.[1,2] Most of the original tanks were of a single-shell construction and at the Hanford site 67 of 177 of them have leaked to date, releasing 3800 m^3 of highly caustic waste (contaminated primarily with the fission products ^{137}Cs, ^{90}Sr, and ^{129}I) into the surrounding vadose zone soils.[2–5] The interactions of these cations with the clay minerals and zeolites in the soils are not well understood, but must be identified in order to generate accurate predictive models of environmental fate.

One method that can provide a molecular-scale analysis of cation/mineral interactions in complex multiphase systems is solid-state nuclear magnetic resonance (NMR). NMR can provide information regarding the electronic structure about each nucleus, coordination numbers, internuclear distances, and information on defects in crystal structures.[6–9] Studies of strontium ($I=9/2$) with solid-state NMR have been limited, primarily due to intrinsic magnetic resonance properties of this nucleus such as a low gyromagnetic ratio (-1.163×10^7 1/T·s), low natural abundance of the NMR-active isotope ($\sim$7% ^{87}Sr), and large quadrupolar coupling constants (9–25 MHz).[9–11] Sensitivity is therefore a major experimental concern. The quadrupolar and chemical shift parameters have been published based on NMR measurements for strontium in only four compounds.[9–11] An attempt to improve the sensitivity of strontium NMR measurements has been made in a single publication, when Larsen and colleagues used the quadrupolar Carr-Purcell-Meiboom-Gill (QCPMG) pulse sequence to study strontium nuclei in strontium nitrate and strontium molybdenate.[10] Before detailed characterization of strontium can be performed with NMR in environmentally relevant samples, a better understanding of strontium behavior in crystalline compounds must be developed.

MAS NMR is a commonly used method to enhance sensitivity and improve the resolution of multiple unique electromagnetic environments about target nuclei in solid samples. In MAS NMR, a powder sample is mechanically rotated about the angle $\theta_m=\cos^{-1}(1/\sqrt{3})\approx54.74°$ with respect to the external magnetic field causing all crystallites in the sample to appear on average to be oriented at this angle with respect to the external magnetic field.[12–14] The net result of this motion is that terms that transform as second-rank tensors (the anisotropic interactions) are modulated so that they provide an averaged contribution to the NMR spectrum.[13] If the spinning rate exceeds the static linewidth of the sample, all of the intensity will be concentrated in a single peak, maximizing the resolution of multiple chemical environments. If the spinning rate does not meet this criterion, the intensity from a broad static line is then collapsed into narrow peaks separated in the frequency domain by integer multiples of the rotational frequency, still providing significant gains in sensitivity.

The quadrupolar interaction, which occurs between a nonuniform charge distribution (such as found in the ^{87}Sr nucleus) and a surrounding electric field gradient (efg), can significantly broaden a resonance and limit the effectiveness of MAS NMR. However, NMR measurements are extremely sensitive to variations in symmetry of the environment surrounding the nuclei of interest, and in perfectly symmetric crystal systems the efg at the cation sites is zero. Therefore, a MAS NMR spectrum of an ensemble of quadrupolar nuclei in a symmetric crystal will contain only one narrow peak for each unique strontium environment in the sample.[15] Despite this fact, many cubic crystals that contain quadrupolar nuclei display a spinning sideband manifold under MAS conditions. These spinning sidebands result from the outer satellite tran-

sitions, which are affected to first order by the quadrupolar interaction arising from variations in the electric field gradient due to defects in the crystal structure, as proposed by Cohen.[15–18] These defects can be dislocations or point defects, which produce variations in the efg by disrupting the symmetry of the crystal.[16] Analyses of the sideband manifold can provide information about the efg distribution in the crystal system and therefore information about the defects in the crystal structure.[15]

Wadkins and Pound were the first authors to make use of NMR to study defects in ionic crystals, specifically the effect of applied homogeneous strain on static spectra of the ^{79}Br, ^{81}Br, and ^{127}I resonances of KBr and KI.[19] Kannert and colleagues also investigated the defects of alkali-halide crystals with NMR and the line shapes that result under each type of defect (point defects, dislocation dipoles, dislocations).[17] Similar MAS NMR methods were used to examine aluminum nuclei dissolved in a rutile (TiO_2) matrix and their proximity to defect sites.[20] Of particular interest to the field of solid-state NMR, crystal defects have been shown to be responsible for the sideband pattern that makes KBr a useful sample for setting the magic angle (utilizing either ^{79}Br or ^{81}Br MAS NMR).[21] Numerous authors have made use of NMR to study defects in semiconductor materials,[15,22–25] and Han *et al.* used a MAS NMR sideband analysis to calculate the efg distribution due to point defects in group III-V semiconductors.[15] Other authors have examined the dislocation dynamics of defects through NMR spectroscopy.[26–28] In this work, we present the first MAS NMR investigation of strontium in cubic and other highly symmetric crystal systems and report the efg distribution about strontium nuclei in SrO, $SrCl_2$, and SrF_2.

THEORY

The quadrupolar interaction measured in a high-field NMR experiment occurs between a nucleus with a nonspherically symmetric charge distribution and the surrounding electric field gradient. The effect of this interaction on the NMR time domain signal can be found by tracing the evolution of an ensemble of nuclear spins under the quadrupolar Hamiltonian, which in Cartesian coordinates is represented by

$$H_q = \vec{I} \cdot \bar{\bar{Q}} \cdot \vec{I}, \tag{1}$$

$$\bar{\bar{Q}} = \frac{eQ}{2I(2I-1)} \bar{\bar{V}}, \tag{2}$$

where Q is the nuclear electric quadrupole moment, e is the charge on an electron, I is the spin quantum number of the quadrupolar nucleus, and $\bar{\bar{V}}$ is the electric field gradient tensor.[29] In the case of perfect cubic crystals (octahedral symmetry) or fluorite analogues (eight—coordinate cubic symmetry), the distribution of local electric charge around a site in the crystal has a high enough symmetry that the efg at every site would be zero, negating any measurable quadrupolar interaction.

In practice, crystals have a distribution of point defects and/or dislocations within their structure.[16] The influences of these defects on an NMR spectrum have been rigorously described by Cohen and Reif, and will be summarized briefly herein.[16] When a defect is proximal to a quadrupolar nucleus, the distribution of electrons about the nucleus is distorted, producing a small local efg and therefore a small local quadrupolar interaction. It is known that imperfect cubic crystal systems in fact produce a distribution of quadrupolar couplings based on the number of defects and distance between defects in the crystal. Cohen and Reif show that if the number of defects in the crystal structure is large, an appreciable efg is felt by nearly all the quadrupolar nuclei of interest. This causes larger quadrupolar couplings (usually characterized by the quadrupolar coupling constant, $C_q = e^2qQ/h$) at the nuclei of interest manifested as a second order quadrupolar broadening and frequency shift of the central transition and first order quadrupolar broadenings that cause the satellite transitions to be too broad for detection by conventional methods. If a small number of defects are present in the sample, the quadrupolar couplings are small and the impact of this efg distribution can be shown to be observable only in the first order quadrupolar interactions of the satellite transitions. In this case, the distribution of efgs can be mapped by integrating the sideband intensities and plotting the integrated intensity against the frequency shift.[15]

Cohen and Reif showed that when small concentrations of defects are present, the shape of each of the satellite transitions is described by[16,18]

$$g(v) = \frac{1}{\pi} \frac{\Gamma}{\Gamma^2 + v^2} \quad \text{for } v < v_c, \tag{3}$$

where

$$\Gamma = \left(\frac{4\pi^2}{9\sqrt{3}} \right) NCv_C \tag{4}$$

and

$$v_C = (2m-1) \left(\frac{3e^2qQ}{4I(2I-1)h} \right). \tag{5}$$

Here Γ is the full width at half-height (FWHH) of the resulting resonance line, eq corresponds to the electric field gradient (rigorously, eV_{zz} where V_{zz} is the z component of the electric field gradient tensor), m is defined based on the transition $m \rightarrow m-1$ corresponding to the satellite transition of interest, v is the independent variable (frequency in this case), N is the number of defects per unit volume, C is a multiplication factor, and the other parameters are defined as for Eq. (2). Note that the expression for the line shape takes the form of a Lorentzian distribution function.

In order to map the efg distribution over the entire sample from the series of spinning sidebands, we must calculate the width of the Lorentzian function corresponding to the sum of all the satellite transitions ($\bar{\Gamma}_m$), which can be accomplished by replacing $(2m-1)$ in the expression for v_c with a weighting factor related to the relative probability of each transition, $\overline{(2m-1)}$. If this is the case, the resulting linewidth is related to the number of defects per unit volume in the sample by

$$\bar{\Gamma}_m = |\overline{2m-1}| \frac{4\pi^2}{3\sqrt{3}} \frac{NCe^2qQ}{4I(2I-1)h}, \quad (6)$$

where $\bar{\Gamma}_m$ is the full width at half-height of the Lorentzian distribution that results from fitting a Lorentzian to the integrated intensities of each sideband, $|\overline{2m-1}|$ is a weighting factor related to the relative probability of an $m \leftrightarrow m-1$ $(m \neq \frac{1}{2})$ transition, and N, C, e, q, and Q are defined as before.[18] In principle, with this equation one can calculate the number of defect sites in a sample from the FWHH of the resulting sideband fit. Unfortunately, only the product NC can be calculated from the Lorentzian fit without prior knowledge of the C values of the sample, which require similar experimentation with samples of known defect number density N.[15]

EXPERIMENT

Strontium oxide (99.9% metals basis) and anhydrous strontium chloride (99.99+%) were obtained from Sigma-Aldrich. Strontium fluoride (99% metals basis) was obtained in its anhydrous form from Alpha Aesar. As these chemicals are moisture sensitive, they were stored under vacuum in a desiccator. Samples were packed and sealed in 5 mm (outer diameter) pencil-type MAS rotors under argon in a sealed glove bag before performing NMR experiments, thereby minimizing exposure to atmospheric water.

MAS echo experiments were performed on both a Varian/Chemagnetics wide-bore Infinity 11.74 T NMR spectrometer (^{1}H resonance frequency of 500 MHz) using a 5 mm triple resonance MAS probe, and a home-built Tecmag Libra 9.4 T instrument (^{1}H resonance frequency of 400 MHz) using a second 5 mm triple resonance MAS probe. The low channels of each probe were tuned to the strontium resonance frequencies of 21.662 MHz and 17.333 MHz at 11.74 and 9.4 T, respectively. Echo experiments of the θ- τ_1- 2θ- τ_2- *acquire* variety were implemented to eliminate the effects of acoustic probe ringing on the NMR spectra while maximizing signal intensity.[30] All spectra were referenced to the ^{87}Sr resonance from a 1 M aqueous solution of $SrCl_2$. In each MAS experiment, the delays (τ_1 and τ_2) were adjusted so as to synchronize the experiment with the rotor period and to ensure the collection of the echo maximum.

At 11.7 T, spectra were collected at a spin rate of 8 kHz with corresponding delays of $\tau_1 = 116$ μs and $\tau_2 = 106$ μs. A central transition selective 90° pulse width of 4.4 μs was found for the solid samples from the liquid 90° pulse width by assuming a scaling of nutation frequency by $I+\frac{1}{2}$. Either 4096 or 8192 data points were collected in each acquisition while sampling every 5 μs. The spectrum for SrO is an average of 10 240 scans while 40 960 scans were acquired for SrF_2 and $SrCl_2$.

MAS experiments at two spin rates were performed at 9.4 T; 8 kHz to confirm the absence of second order quadrupolar effects through comparison of the peak shifts of the resonance line at both fields and at 5 kHz ($\tau_1 = 196$ μs, $\tau_2 = 186$ μs) to generate a greater number of spinning sidebands to facilitate a more accurate estimation of the efg distribution. Experiments at this field were acquired with a central transition selective 90° pulse width of 4 μs and a 600 kHz sweep width. The oxide and chloride spectra at both spin rates are an average of 61 440 acquisitions with 16 384 points collected each acquisition cycle. Based on an observed reduction in signal to noise of the fluoride sample at 11.7 T, 153 600 acquisitions were collected for this sample at 9.4 T, again with 16 384 data points per acquisition cycle. A Bloch-decay experiment at 5 kHz employing sufficient acquisition delays to remove ringing effects was also run for the $SrCl_2$ sample to test the quantitative accuracy of the integrations determined from echo experiments.

All spectra were processed by phasing the free induction decay (FID) and left shifting data points until the echo maximum was reached as the first data point in the "real" quadrature channel. Exponential apodizations in the time domain equivalent to 50 Hz of Lorentzian broadening were applied to each data set. The sideband intensities were integrated by least-squares iterative fitting with Lorentzian functions to each sideband using the program DMfit by Massiot *et al.*[31] Electric field gradient distributions were determined by plotting the integrated intensity of each sideband as a function of frequency and, as suggested in Han *et al.*,[15] a least-squares fit of these data with a Lorentzian line shape performed here with Origin software. The resonance lines for the 8 kHz data at both field strengths were also analyzed in DMfit to extract the peak position. From the peak shifts at two fields, one can in principle calculate the isotropic chemical shift and quadrupolar product $[P_q = C_q\sqrt{1+(\eta^2/3)}]$ so as to confirm the existence of negligible second-order quadrupolar effects.

RESULTS AND DISCUSSION

Strontium oxide has a simple cubic crystal structure in its anhydrous form and, therefore, an ideal crystal would contain strontium in a symmetric six-coordinate environment with a $C_q \approx 0$.[32] Figure 1 displays the MAS NMR results from both field strengths for SrO. The well-defined sideband manifold at an 8 kHz spin rate can clearly be seen and covers roughly 3000 ppm for the 11.74 T data and around 4500 ppm for the 9.4 T data. This reduction in overall width accompanying the increase in field strength from 9.4 T to 11.74 T is in agreement with theory, in which the static linewidth due to the quadrupolar interaction scales inversely with applied magnetic field strength. It is also apparent by observation that there is little shift in the position of the resonance line due to a second order quadrupolar shift (340.4±1.2 ppm at 11.74 T vs 339.8±0.6 ppm at 9.4 T), implying that the overall quadrupolar coupling constant for the strontium nuclei in our SrO sample is small and the concentration of defects is low. In fact, when P_q is calculated for SrO based on the observed difference in chemical shift between the two fields, a value of 0.6 MHz is obtained. This is below the P_q value calculated for the uncertainty of the measured shift alone, rendering the experimental P_q statistically insignificant. The

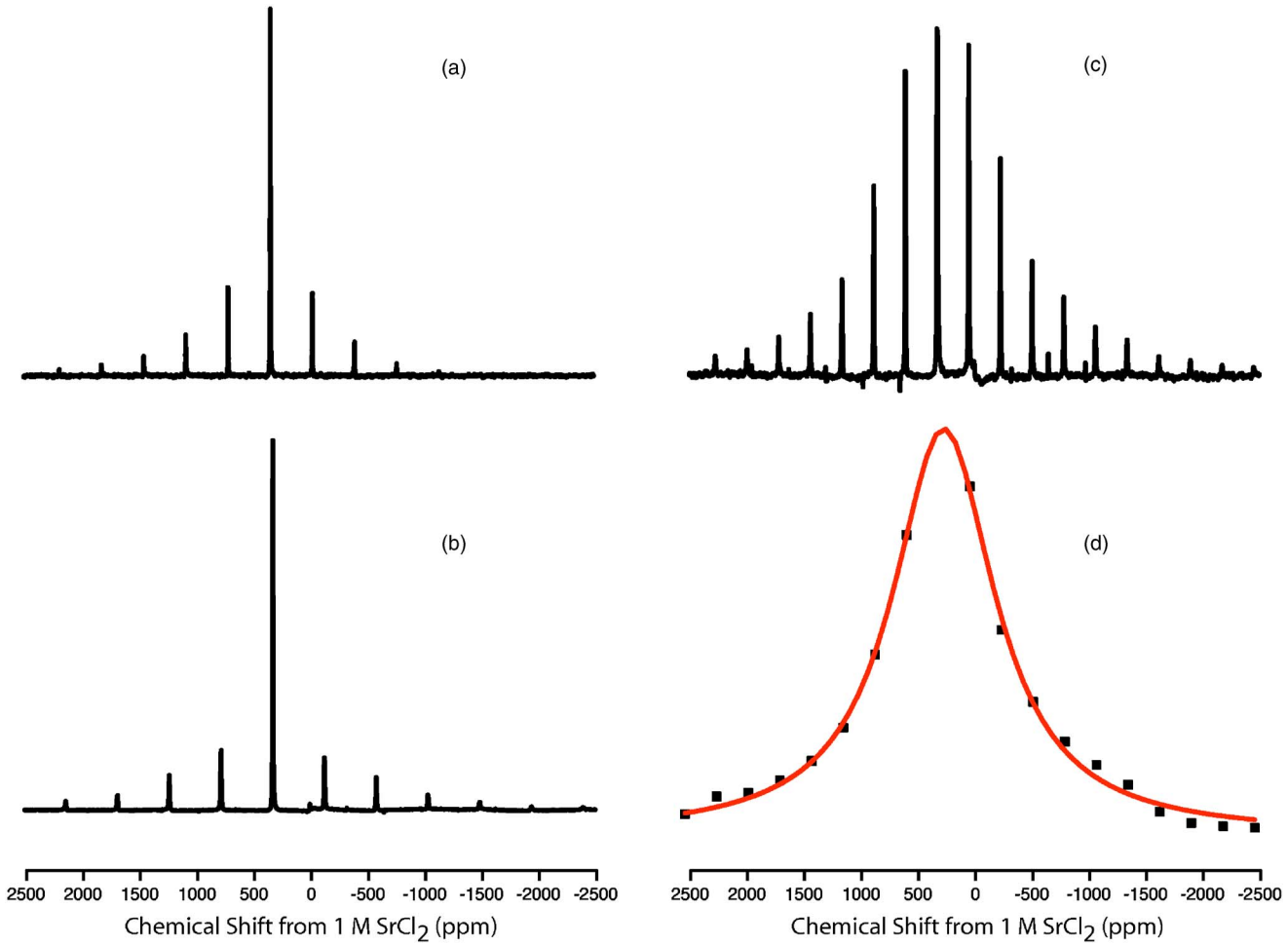

FIG. 1. (Color online) ^{87}Sr MAS NMR spectra of SrO. Spectra obtained with (A) an 8 kHz spin rate at 11.7 T and (B) an 8 kHz spin rate at 9.4 T show little shift in the resonance line, indicating no appreciable second-order quadrupolar character. Parts (C) and (D) contain the spinning sideband spectrum from the 5 kHz spin rate (scaled to maximize the appearance of sidebands with center band cutoff) and resulting efg distribution, respectively.

lack of second-order quadrupolar character was further confirmed by iterative fitting of the resonance line shape, which has clearly defined Lorentzian character rather than a MAS quadrupolar shape, and the best-fit Lorentzian line is centered at ~340 ppm at 9.4 T. It is also clear that little spin exchange is occurring for strontium at room temperature as the line shape would be Gaussian in character if the exchange was appreciable.[33,34] Since the resonance line lacks significant second-order quadrupolar character and the sideband pattern lacks sharp edges associated with quadrupolar patterns, we can conclude that the sideband manifold is a result of a distribution of efgs caused by a small concentration of defects. The integrated sideband intensities from the 5 kHz MAS data are well fit by a Lorentzian function (R^2 =0.9939), as expected for a small number of defects. The characteristics of the efg distribution (FWHH) for strontium oxide and the other compounds are compiled in Table I along with the isotropic chemical shifts for each sample.

Strontium chloride shares the fluorite (CaF_2) structure, so that in the ideal case the strontium atoms sit in the center of a cube made up of eight chlorine atoms in a uniformly symmetric arrangement.[35] In a perfect crystal, this arrangement will also produce an efg of zero about the strontium nuclei, yielding a resonance free of second-order quadrupolar effects. Indeed, the resonance line can be observed to shift very little between the two field strengths (46.2±1.2 ppm at 11.74 T vs 45.4±0.6 ppm at 9.4 T) and lacks any substantial second-order quadrupolar character (Fig. 2). This implies a relatively small concentration of defect sites in the strontium chloride sample. The resonance line is again well fit by a Lorentzian function, indicating no spin exchange at room temperature. The sideband intensities of the strontium chloride sample are fit closely by a Lorentzian distribution (R^2 =0.9987), again indicating a small concentration of defects as the source of the first order quadrupolar broadening. This

TABLE I. Chemical shift and efg distribution parameters.

Sample	δ_{iso} (ppm)	FWHH efg distribution (kHz)	R^2 efg distribution
SrO	340±1	50.4±2.5	0.9939
$SrCl_2$	45.9±1.2	30.9±1.4	0.9987
SrF_2	−13.0±1.2	104±18	0.9508

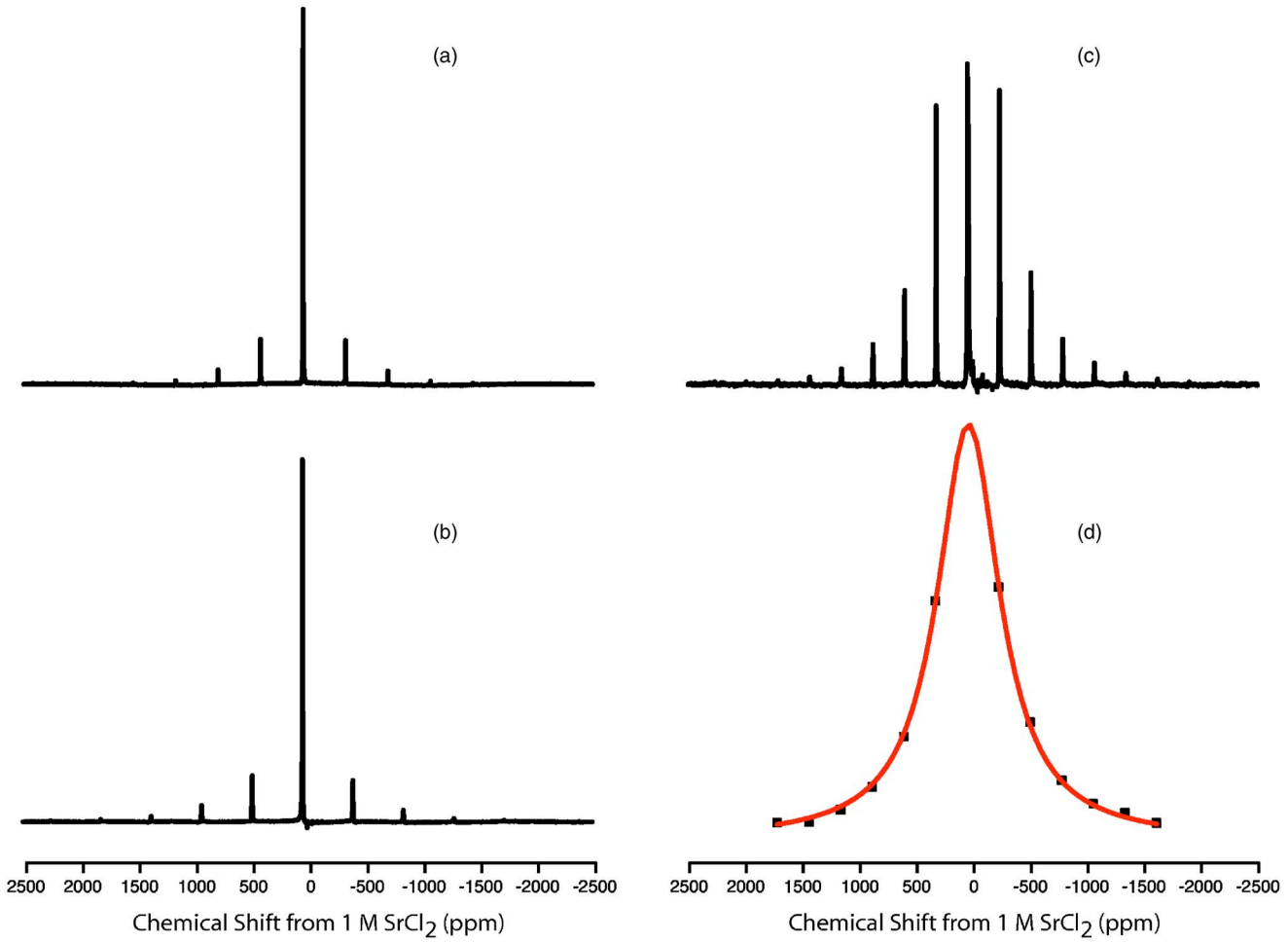

FIG. 2. (Color online) ^{87}Sr MAS NMR spectra of $SrCl_2$. Parts (A) and (B) contain the 8 kHz spin rate spectra at 11.7 T and 9.4 T (respectively). These again show negligible shift in the resonance line and a sideband manifold without sharp edges. Parts (C) and (D) contain the spinning sideband spectrum from the 5 kHz spin rate (scaled to maximize the appearance of sidebands with center band cutoff) and resulting efg distribution for $SrCl_2$, respectively.

distribution has a much narrower width than that found for the strontium oxide sample (30.9 ± 1.4 kHz vs 50.4 ± 2.5 kHz), which may indicate the presence of fewer defects in the strontium chloride. In order to clearly reach this conclusion, the value of eq arising from the defect sites in each material must be known and studies must be performed with samples of known N in order to determine the value of C for each of the strontium samples.

The signal-to-noise (S/N) ratio obtained from similar experiments performed on a strontium fluoride sample, which also possesses the fluorite structure,[36] is much lower than that measured for either the oxide or chloride samples. The precise reason for this discrepancy is unknown at this time. MAS NMR at 8 kHz produces a sideband manifold displaying the characteristics of an efg distribution based on a small defect concentration (Fig. 3). This can be seen more clearly in the data from the 9.4 T instrument, in which a larger number of acquisitions were obtained to overcome the discrepancy in sensitivity. Again, the resonance line does not shift appreciably between the two field strengths (-12.3 ± 1.2 ppm at 11.74 T vs -13.6 ± 0.6 ppm at 9.4 T) and is well fit with a Lorentzian. The sideband pattern is similar to that displayed by strontium oxide, though the intensities from the strontium fluoride 5 kHz sidebands do not provide as good a match to the Lorentzian distribution function expected for a point defect-based efg distribution as for SrO or $SrCl_2$. The higher degree of scatter in the sideband intensity plot is likely a function of the difficulty in accurately estimating the peak areas at this S/N ratio. The FWHH of the fluoride is much larger than either the chloride or oxide samples, which may indicate that strontium fluoride has the greatest number of defect sites per unit volume depending on the values of eq and C for the three materials.

CONCLUSIONS

This paper presents the first MAS NMR study of strontium, focusing on crystalline samples with symmetric electron environments around the strontium nuclei. In each sample studied, the NMR spectra featured a sharp peak and a manifold of spinning sidebands that lacked features associated with quadrupolar powder patterns. The chemical shifts of the resonance line at two fields were within the uncertainty of the shift measurements and were well fit by a

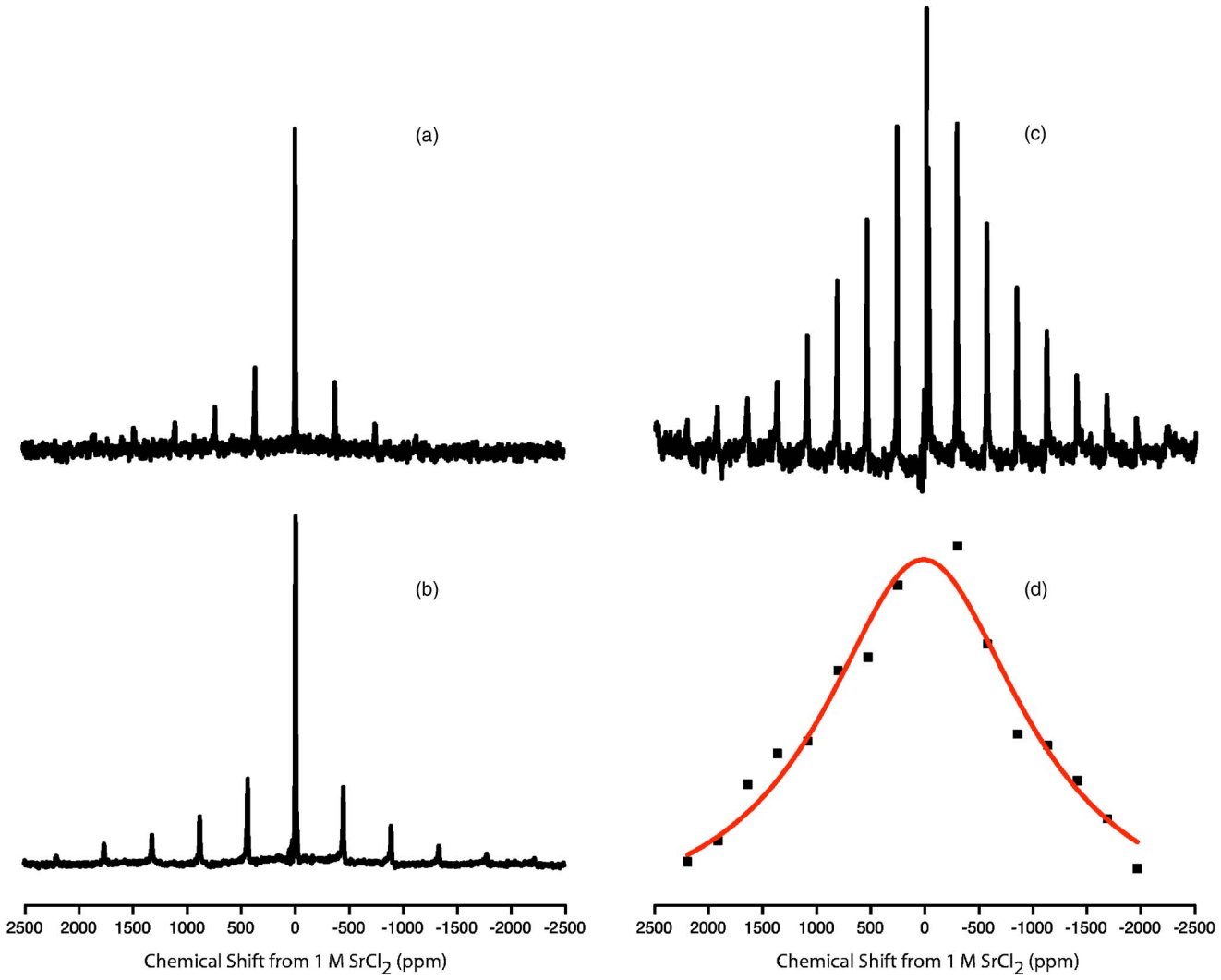

FIG. 3. (Color online) ^{87}Sr MAS NMR spectra of SrF_2. Parts (A) and (B) contain the 8 kHz spin rate spectra at 11.7 T and 9.4 T (respectively). Note the reduction in signal-to-noise ratio for (A) versus the other spectra from 11.7 T. Significantly more sidebands are visible in the results from 9.4 T where a greater number of acquisitions were made. It can be seen that no appreciable second order quadrupolar character exists for this sample. Parts (C) and (D) contain the spinning sideband spectrum from the 5 kHz spin rate (scaled to maximize the appearance of sidebands with center band cutoff) and resulting efg distribution for SrF_2, respectively.

Lorentzian function, demonstrating that there are negligible second-order quadrupolar interactions for strontium in these systems. These observations are consistent with crystal systems that contain a low concentration of defects in their crystal structure. The electric field gradient distributions due to defects in the structure were calculated according to the method of Han *et al.* for low-defect crystalline materials. Further studies are necessary to determine C and enable the calculation of the number of defects N directly from the NMR results.

ACKNOWLEDGMENTS

The authors would like to acknowledge Dr. Alan Benesi and John Lintner of The Pennsylvania State University NMR facility for assistance in implementing strontium NMR. One of the authors (G.M.B.) would also like to acknowledge Professor Clare Gray for useful comments that prompted the quantitative analyses of these data. This research was supported by the U.S. Department of Energy, Environmental Management Sciences Program Grant No. DE-FG07-99ER15012.

*Author to whom correspondence should be addressed. Electronic address: ktm2@psu.edu

[1] T. E. Marceau, D. W. Harvey, D. C. Stapp, S. D. Cannon, C. A. Conway, D. H. Deford, B. J. Freer, M. S. Gerber, J. K. Keating, C. F. Noonan, and G. Weisskopf, Hanford Cultural and Historic Resources Program, United States Department of Energy, Richland, 2002.

[2] R. J. Serne, J. M. Zachara, and D. S. Burke, PNNL-11495 UC-510, 1998.

[3] J. M. Zachara, S. C. Smith, C. X. Liu, J. P. McKinley, R. J. Serne, and P. L. Gassman, Geochim. Cosmochim. Acta **66**, 193 (2002).

[4] J. F. Ahearne, Phys. Today **50**, 24 (1997).

[5] J. P. McKinley, C. J. Zeissler, J. M. Zachara, R. J. Serne, R. M. Lindstrom, H. T. Schaef, and R. D. Orr, Environ. Sci. Technol. **35**, 3433 (2001).

[6] H. M. Liu, H. M. Kao, and C. P. Grey, J. Phys. Chem. B **103**, 4786 (1999).

[7] F. G. Vogt, D. J. Aurentz, and K. T. Mueller, Mol. Phys. **95**, 907 (1998).

[8] C. A. Fyfe, K. C. Wongmoon, Y. Huang, H. Grondey, and K. T. Mueller, J. Phys. Chem. **99**, 8707 (1995).

[9] T. J. Bastow, Chem. Phys. Lett. **354**, 156 (2002).

[10] F. H. Larsen, J. Skibsted, H. J. Jakobsen, and N. C. Nielsen, J. Am. Chem. Soc. **122**, 7080 (2000).

[11] M. J. Weber and R. R. Allen, J. Chem. Phys. **38**, 726 (1962).

[12] D. Doskocilova and B. Schneider, Chem. Phys. Lett. **6**, 381 (1970).

[13] U. Haeberlen and J. S. Waugh, Phys. Rev. **175**, 453 (1968).

[14] E. R. Andrew, S. Clough, L. F. Farnell, T. D. Gledhill, and I. Roberts, Phys. Lett. **21**, 505 (1966).

[15] O. H. Han, H. K. C. Timken, and E. Oldfield, J. Chem. Phys. **89**, 6046 (1988).

[16] M. H. Cohen and F. Reif, in *Solid State Physics: Advances in Research and Applications*, edited by D. Turnbull and F. Seitz (Academic, New York, 1957), Vol. 5, p. 321.

[17] O. Kanert, D. Kotzur, and M. Mehring, Phys. Status Solidi **36**, 291 (1969).

[18] M. H. Cohen, Philos. Mag. **3**, 564 (1958).

[19] G. D. Watkins and R. V. Pound, Phys. Rev. **89**, 658 (1953).

[20] J. F. Stebbins, I. Famaon, and U. Klabunde, J. Am. Ceram. Soc. **72**, 2198 (1989).

[21] J. S. Frye and G. E. Maciel, J. Magn. Reson. (1969-1992) **48**, 125 (1982).

[22] M. Suemitsu and N. Nakajo, J. Appl. Phys. **66**, 3178 (1989).

[23] R. K. Hester, A. Sher, J. F. Soest, and G. Weisz, Phys. Rev. B **10**, 4262 (1974).

[24] J. F. Hon and P. J. Bray, Phys. Chem. Solids **11**, 149 (1959).

[25] P. E. Stallworth, J. B. d'Espinose de la Caillerie, J. Maquet, F. Babonneau, J. F. Guillemoles, M. Powalla, V. Lyakovitskaya, M. Yakushev, and B. Tomlinson, Thin Solid Films **387**, 235 (2001).

[26] J. P. Yesinowski and A. P. Purdy, J. Am. Chem. Soc. **126**, 9166 (2004).

[27] Z. H. Xie, M. E. Smith, J. H. Strange, and C. Jaeger, J. Phys.: Condens. Matter **7**, 2479 (1995).

[28] J. T. M. De Hosson, Dislocation solids, Proceedings of the Yamada Conference, 9th, 1985, p. 261.

[29] C. P. Slichter, *Principles of Magnetic Resonance* (Springer-Verlag, Berlin, Heidelberg, 1990).

[30] E. Oldfield and R. J. Kirkpatrick, Science **227**, 1537 (1985).

[31] D. Massiot, F. Fayon, M. Capron, I. King, S. Le Calve, B. Alonso, J.-O. Durand, B. Bujoli, Z. Gan, and G. Hoatson, Magn. Reson. Chem. **40**, 70 (2002).

[32] T. A. Wilson, Phys. Rev. **31**, 1117 (1928).

[33] M. A. Ruderman and C. Kittel, Phys. Rev. **96**, 99 (1954).

[34] J. H. Van Vleck, Phys. Rev. **74**, 1168 (1948).

[35] H. Ott, Z. Kristallogr., Kristallgeom., Kristalphys., Kristallchem. **63**, 222 (1926).

[36] A. Ferrari, Atti III Congr. Naz. Chim. Pura Appl. **1930**, 452 (1930).